
Improving Spatio-Temporal Residual Error Propagation by Mitigating Over-Squashing

Seyed Mohamad Moghadas^{1,2}, Esther Rodrigo Bonet^{1,2}, Bruno Cornelis, Adrian Munteanu^{1,2*}

¹ ETRO Department, Vrije Universiteit Brussel, B-1050 Brussels, Belgium

² imec Kapeldreef 75, B-3001 Leuven, Belgium

Seyed.Mohamad.Moghadas, Esther.Rodrigo.Bonet, Adrian.Munteanu@vub.be

Abstract

Residual error propagation remains a fundamental problem in recurrent models, where small prediction inaccuracies compound over time and degrade long-horizon performance. Accurately modeling the correlation structure of such residuals is critical for reliable uncertainty quantification in probabilistic multivariate time-series forecasting. While recent time-series deep models efficiently parametrize time-varying *contemporaneous* correlations, they often assume temporal independence of errors and neglect spatial correlation across the observed network. In this paper, we introduce Teger, a structured uncertainty module that overcomes the spatial and temporal limitations of error-correlated autoregressive forecasting. Teger proposes a spatial curvature-aware graph rewiring mechanism explicitly strengthening information-bottleneck edges identified by discrete Forman curvature. The component is integrated into a low-rank-plus-diagonal covariance head, preserving tractable inference via the Woodbury identity. Teger is backbone-agnostic, requiring only the latent state produced by any autoregressive encoder. We provide theoretical evidence of Teger, and experimentally evaluate it on LSTM, Transformer, and xLSTM backbones across four real-world spatio-temporal datasets, showing consistent improvement in Continuous Ranked Probability Score (CRPS). We further provide a formal theoretical analysis connecting curvature-aware rewiring to (i) oversquashing alleviation, (ii) improved spectral connectivity, (iii) reduced effective resistance, and (iv) improved covariance calibration bounds. Repo

1 Introduction

With the rapid development of Intelligent Transportation Systems (ITS), traffic forecasting has become a fundamental component of modern urban infrastructure. Accurate forecasting enables informed traffic management, congestion mitigation, and route planning [10]. Recent advances in deep learning have significantly improved the modeling of complex spatio-temporal dependencies in ITS, particularly through graph neural networks (GNNs). Yet, most approaches focus primarily on predicting point estimates [5, 21, 27, 28, 19, 20, 16], while modeling uncertainty remains comparatively underexplored. In practice, empirical evidence reveals pronounced spatiotemporal covariance patterns in traffic residuals: predictions at one sensor can be strongly influenced by upstream and downstream conditions, leading to correlated residuals across the network (Figure 5b). Despite this, existing methods rarely capture such structure. And even when covariance is modeled, it is typically restricted to the temporal dimension, thereby failing to fully capture their spatial interaction. For instance, TCVAR [29] explicitly models the temporal covariance, but does not extend this modeling across space. Beyond covariance structure, these models also struggle to explicitly capture volatility, leading to miss-calibrated uncertainty estimates [18]. On top, most methods are restricted to specific autoregressive backbones, limiting in flexibility and applicability.

*Senior IEEE Member

The inability to capture spatio-temporal covariance is intrinsically linked to the over-squashing phenomenon in GNNs, where long-range dependencies are excessively compressed into bounded representations, degrading information propagation across the traffic graph. In recent years, OQ has received increasing attention in the graph learning community [22, 1], with works focusing on classical tasks such as node classification and edge prediction. Two families of remedies, both operating inside the message-passing layer of GNNs, are now well-established. *Curvature-based rewiring*, introduced by SDRF [22] and subsequently refined, identifies bottleneck edges through discrete Ricci-style curvature and adds or removes edges to relieve them. Alternatively, *sequential structural rewiring*, exemplified by LASER [3], constructs a sequence of augmented graph snapshots that add long-range shortcuts while explicitly trading off connectivity, locality, and sparsity.

[13] extends the notion to spatio-temporal networks and establishes a theoretical foundation. Counter-intuitively, their analysis shows that convolutional spatiotemporal graph neural networks (STGNNs) favor information propagation from temporally distant nodes over closer ones. However, they do not formalize the effect of OQ mitigation on predictive performance, and neither their work nor prior work explores it in the context of dynamic graphs, to the best of our knowledge. However, we argue that spatio-temporal forecast errors do not occur in isolation: they propagate across the network’s dynamic structure following its underlying topology, and this propagation is both time-varying and influenced by latent system states (Fig. 5). Capturing this structure is, at heart, a covariance-modeling problem on a dynamic graph, and the same bottlenecks that distort message passing also distort the spatial covariance of residuals—concentrating dependence along thin chains and underestimating cross-region correlation. In this work, we address these gaps through a backbone-agnostic, parametric, probabilistic framework for spatio-temporal networks such as road graphs. We provide a theoretical analysis linking OQ alleviation to improved spectral connectivity and reduced effective resistance, and show how these properties lead to enhanced predictive performance by mitigating residual error propagation.

We propose **Teger**, a backbone-agnostic probabilistic framework for spatio-temporal forecasting on dynamic graphs that places a curvature-aware spatial covariance inside a low-rank-plus-diagonal noise head. In contrast to LASER [3], which *adds* edges via a sequence of augmented snapshots, and to SDRF [22], which adds and removes edges based on Balanced Forman curvature, Teger keeps the input topology fixed and only *reweights* existing edges using the same Balanced Forman signal. This is, deliberately, a weaker structural intervention: it cannot create long-range pathways where none exist, but it preserves locality and sparsity by construction, sidesteps the connectivity-locality-sparsity trade-off that motivates LASER’s sequential design, and—most importantly for our setting—admits a closed-form low-rank projection that integrates cleanly into a Woodbury-style covariance update. The contribution of Teger is therefore a new curvature-aware reweighting algorithm and at the same time a probabilistic-forecasting counterpart to the existing OQ-mitigation literature.

Our contributions are four-fold: (1) A dynamic low-rank-plus-diagonal covariance model for spatio-temporal residuals, capturing spatial dependence through graph-aware latent factors and temporal dependence through an autoregressive structure on the residual process. (2) A curvature-based spatial correlation mechanism modeling error diffusion on the dynamic graph, with state-aware dynamics and volatility adaptation. (3) A curvature-aware edge-reweighting step embedded inside the covariance head, together with a learnable low-rank projection that maps the rewired Laplacian into an R -dimensional factor space at $\mathcal{O}(R^3)$ rather than $\mathcal{O}(N^3)$ cost. To our knowledge, this is the first integration of curvature-based rewiring into a probabilistic spatio-temporal forecaster. (4) Integration of these components into a unified probabilistic autoregressive framework that preserves computational tractability while materially expanding the expressiveness of spatio-temporal uncertainty modeling.

We are explicit about the scope of the OQ-mitigation claim: edge reweighting is a strictly weaker tool than the structural rewirings of LASER and SDRF, and it can relieve over-squashing only in regimes where bottleneck edges are present but underweighted—a regime we argue is well-matched to road-network forecasting, where the physical road graph is essentially fixed but edge importances vary in time. We discuss when this regime applies in Section 4.3.

The paper is structured as follows. Section 2 overviews the related work. Section 3 presents the proposed methodology and performance figures used to compare the proposed spatial curvature-aware graph reweighting mechanism against the state of the art. Section 4 reports and analyses the experimental results. Section 5 draws the conclusions.

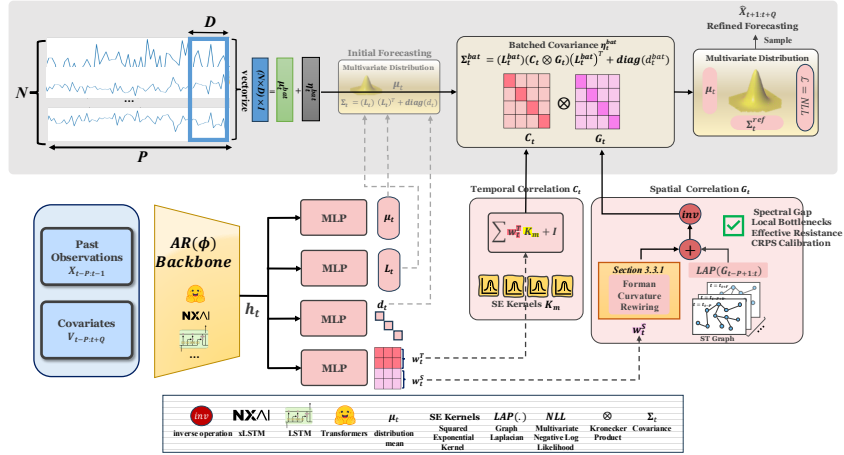


Figure 1: Overview of Teger. An autoregressive backbone encodes past observations into a latent state h_t . MLP heads produce the predictive mean and an initial low-rank-plus-diagonal (LRD) covariance. The temporal kernel mixture C_t and graph-based spatial factor covariance G_t are combined into a Kronecker batch covariance, which enables inference-time residual refinement and yields calibrated predictions.

2 Related Work

Neural time-series forecasting. Traffic forecasting with deep learning is a rapidly developing research area [5]. While spatial (CNN-based) [21, 27] and recurrent (RNN-based [28] and LSTM-based models [19, 20]) models have been proposed, we review transformer-based models due to their powerful ability in extracting spatio-temporal features and their effectiveness in few-shot learning scenarios. Inspired by the vanilla transformer mechanism introduced in [23], PatchTST [16] highlights the importance of extracting local semantic information from time series data, often overlooked by models that use point-wise tokens and then re-process the output of a transformer for a point forecast or a probabilistic forecast. Other works build on the transformer architecture, and propose alternative strategies to the vanilla attention mechanism [14], leading to models better tailored for time-series forecasting [11, 17, 30]. For instance, [14] proposes a spatio-temporal attention model, others leverage trend-aware decomposition in the definition of the attention layer [25, 24, 12, 31, 15, 8]. On the other hand, copula-based transformer models [2], are better at capturing volatilities, defined as the degree of variation in the time-series value over time.

Correlated errors in probabilistic forecasting. Recent research in multivariate probabilistic forecasting [29] has highlighted the limitations of one-step-ahead independent likelihood training, which ignores serial correlations in forecast errors. A tractable remedy is to introduce a latent low-dimensional error process and correlate it within a finite horizon using a dynamic correlation matrix (e.g., kernel-mixture parameterizations) [29]. This constructs a block covariance over a temporal window while maintaining efficient likelihood computation using the Woodbury identity [6] and the matrix determinant lemma. These methods handle temporal correlations only within the residuals, whereas our method additionally captures spatial dependencies across them.

3 Methodology

We pose our probabilistic auto-regressive formulation in Section 3.1, then describe the temporal and spatial error correlation modeling in Sections 3.2 and 3.3. Section 3.4 introduces theoretical performance figures for curvature aware rewiring. Section 3.5 details the sampling performed by the proposed method at inference time. See Fig. 1 for an visual representation of our approach.

3.1 Probabilistic Autoregressive Formulation

Let $\mathbf{x}_t = [x_{1,t}, \dots, x_{N,t}]^\top \in \mathbb{R}^N$ denote the vector of multivariate time series variables at time step t , where N is the number of spatially distributed nodes. The objective of probabilistic spatio-temporal forecasting is to estimate the joint conditional distribution $p(\mathbf{x}_{T+1:T+Q} \mid \mathbf{x}_{T-P+1:T}; \mathbf{v}_{T-P+1:T+Q})$, given the observed history $\{\mathbf{x}_t\}_{t=1}^T$ and time-dependent covariates \mathbf{v}_t . Our methodology employs a multivariate Gaussian distribution as the probabilistic head, decomposing the time series variable as $\mathbf{x}_t = \boldsymbol{\mu}_t + \boldsymbol{\eta}_t$, where $\boldsymbol{\eta}_t \sim \mathcal{N}(\mathbf{0}, \Sigma_t)$ represents the stochastic error component. To efficiently model the covariance matrix Σ_t for large N , we adopt a low-rank-plus-diagonal parameterisation:

$$\Sigma_t = \mathbf{L}_t \mathbf{L}_t^\top + \text{diag}(\mathbf{d}_t), \quad (1)$$

where $\mathbf{L}_t \in \mathbb{R}^{N \times R}$ ($R \ll N$) and $\mathbf{d}_t \in \mathbb{R}_+^N$.

3.2 Temporal Error Correlation Modeling

To capture spatio-temporal dependencies, we extend error modelling over a finite horizon D by stacking residuals: $\boldsymbol{\eta}_t^{\text{bat}} = \text{vec}(\boldsymbol{\eta}_{t-D+1:t}) \in \mathbb{R}^{DN}$. The joint distribution is:

$$\boldsymbol{\eta}_t^{\text{bat}} \sim \mathcal{N}(\mathbf{0}, \Sigma_t^{\text{bat}}), \quad \Sigma_t^{\text{bat}} = \mathbf{L}_t^{\text{bat}} (\mathbf{C}_t \otimes \mathbf{G}_t) (\mathbf{L}_t^{\text{bat}})^\top + \text{diag}(\mathbf{d}_t^{\text{bat}}), \quad (2)$$

where $\mathbf{L}_t^{\text{bat}} = \text{blkdiag}(\mathbf{L}_{t-D+1}, \dots, \mathbf{L}_t) \in \mathbb{R}^{DN \times DR}$, $\mathbf{C}_t \in \mathbb{R}^{D \times D}$ captures temporal correlation, and $\mathbf{G}_t \in \mathbb{R}^{R \times R}$ encodes spatial factor covariance informed by the graph structure.

The temporal correlation matrix \mathbf{C}_t is parameterised as a dynamic kernel mixture, similar to TCVAR:

$$\mathbf{C}_t = \sum_{m=1}^M w_{m,t} \mathbf{K}_m, \quad w_{m,t} \geq 0, \quad \sum_{m=1}^M w_{m,t} = 1, \quad (3)$$

where $\{\mathbf{K}_m\}$ are fixed Positive Semi-Definite (PSD) kernel matrices (e.g., squared exponential with varying length scales) and $\{w_{m,t}\}$ are time-varying mixture weights learned through a softmax network.

3.3 Spatial Correlation Modeling

Motivated by the limitations of existing models such as TCVAR in capturing spatial error propagation, Teger proposes a novel paradigm for spatial error propagation that makes use of a stochastic curvature-aware reweighting approach applicable for ST networks.

3.3.1 Dynamic Curvature-Aware Spatial Correlation

To incorporate spatial dependencies inherent in transportation networks, we introduce a dynamic graph $\mathcal{G}_t = (\mathcal{V}, \mathcal{E}_t, \mathbf{A}_t)$. We consider eigenvalues of the graph Laplacian to be ordered as: $\lambda_n \geq \lambda_{n-1} \geq \dots \geq \lambda_1$. A critical challenge in cross-correlation methods applied to transportation systems is the *oversquashing* phenomenon, where information flow between distant nodes becomes exponentially attenuated through bottleneck edges with highly negative discrete curvature. Based on the theorem from [22], edges (i, j) with Balanced Forman curvature $\kappa(i, j) \leq -2 + \delta$ (for small $\delta > 0$) act as information bottlenecks, severely limiting the influence propagation from node i to its extended neighborhood. To mitigate this, we propose the curvature-aware spatial precision matrix rewiring algorithm (Algorithm 1).

Proposition 1 (Validity of Reweighted Covariance). *Assume the reweighted adjacency \mathbf{W}'_t is symmetric and entrywise nonnegative. Then:*

(i) *The graph Laplacian \mathbf{L}'_t of \mathbf{W}'_t is PSD.*

(ii) *For any $\mathbf{P} \in \mathbb{R}^{N \times R}$, the projected matrix $\mathbf{L}_t^{(R)} = \mathbf{P}^\top \mathbf{L}'_t \mathbf{P}$ is PSD.*

(iii) *For $\alpha > 0$, $\beta \geq 0$, and $\sigma_{\min} > 0$, the precision matrix $\mathbf{Q}_t = \alpha \mathbf{I}_R + \beta \mathbf{L}_t^{(R)} + \sigma_{\min} \mathbf{I}_R$ is symmetric positive definite, and hence $\mathbf{G}_t = \mathbf{Q}_t^{-1}$ is a valid covariance matrix.*

The proof is given in Appendix B.1. Proposition 1 establishes only that the construction yields a well-defined covariance matrix. We now provide a theoretical justification connecting the curvature-aware rewiring to oversquashing alleviation, long-range information flow, and calibration improvement.

Algorithm 1 Curvature-Aware Spatial Precision Matrix Rewiring

```

1: Input: Batch adjacency matrices  $\{\bar{\mathbf{A}}_{b,t}\}_{b=1}^B$ , fixed jitter  $\sigma_{\min} > 0$ 
2: Learned parameters:  $\kappa_0 \in \mathbb{R}, \tau > 0, \lambda > 0, \alpha > 0, \beta \geq 0, \mathbf{P} \in \mathbb{R}^{N \times R}$  ▷ All trained
   end-to-end via back-prop
3: Output: Spatial factor covariance  $\mathbf{G}_t \in \mathbb{R}^{R \times R}$ 
4:  $\mathbf{A}_t \leftarrow \frac{1}{B} \sum_{b=1}^B \bar{\mathbf{A}}_{b,t}$ 
5:  $\mathbf{W}_t \leftarrow \frac{1}{2}(\mathbf{A}_t + \mathbf{A}_t^\top)$ 
6: for each edge  $(i, j)$  in  $\mathbf{W}_t$  do
7:   Compute Balanced Forman curvature  $\kappa_{ij,t}$ 
8:    $b_{ij,t} \leftarrow \text{softplus}(\tau(\kappa_0 - \kappa_{ij,t}))$ 
9: end for
10: for each edge  $(i, j)$  in  $\mathbf{W}_t$  do
11:    $W'_{ij,t} \leftarrow W_{ij,t}(1 + \lambda b_{ij,t})$ 
12: end for
13: Compute graph Laplacian  $\mathbf{L}'_t$  from  $\mathbf{W}'_t$ 
14:  $\hat{\mathbf{P}} \leftarrow \text{colnorm}(\mathbf{P}); \mathbf{L}_t^{(R)} \leftarrow \hat{\mathbf{P}}^\top \mathbf{L}'_t \hat{\mathbf{P}}$ 
15:  $\mathbf{Q}_t \leftarrow (\alpha + \sigma_{\min})\mathbf{I}_R + \beta \mathbf{L}_t^{(R)}; \mathbf{G}_t \leftarrow \mathbf{Q}_t^{-1}$ 
16: return  $\mathbf{G}_t$ 

```

3.4 Theoretical Analysis of Curvature-Aware Reweighting

Throughout this section we work with the *unnormalised* graph Laplacian $\mathbf{L} = \mathbf{D} - \mathbf{W}$ unless explicitly stated otherwise, where $\mathbf{D} = \text{diag}(\mathbf{W}\mathbf{1})$ is the degree matrix. All graphs are assumed to be undirected, weighted, and connected. We write $\mathbf{A} \succeq \mathbf{B}$ to denote the Löwner (positive semidefinite) partial order.

3.4.1 Direction 1: Spectral Gap Improvement

Lemma 2 (Laplacian Monotonicity). *Let $\mathbf{W}, \Delta\mathbf{W} \in \mathbb{R}^{N \times N}$ be symmetric, entrywise non-negative matrices with corresponding unnormalised Laplacians \mathbf{L} and \mathbf{L}_Δ . Then*

$$\mathbf{L}_{\mathbf{W}+\Delta\mathbf{W}} = \mathbf{L}_{\mathbf{W}} + \mathbf{L}_{\Delta\mathbf{W}}, \quad \mathbf{L}_{\Delta\mathbf{W}} \succeq \mathbf{0}. \quad (4)$$

Proposition 3 (Spectral Gap Monotonicity). *Let $\mathbf{L}_t = \text{diag}(\mathbf{W}_t) - \mathbf{W}_t = \mathbf{D}_t - \mathbf{W}_t$ be the unnormalised Laplacian of the original graph and \mathbf{L}'_t the Laplacian of the reweighted graph \mathbf{W}'_t obtained via Algorithm 1. Then:*

(i) $\mathbf{L}'_t \succeq \mathbf{L}_t$ in Löwner order sense.

(ii) If $\mathbf{L}_{\Delta\mathbf{W}_t}$ is positive definite then $\lambda_k(\mathbf{L}'_t) > \lambda_k(\mathbf{L}_t)$ for all k , that is, the inequality is strict.

Remark 4. Proposition 3 is stated for the *unnormalised* Laplacian $\mathbf{L} = \mathbf{D} - \mathbf{W}$, which is the object directly used in Algorithm 1. An analogous result for the *normalised* Laplacian $\tilde{\mathbf{L}} = \mathbf{D}^{-1/2}\mathbf{L}\mathbf{D}^{-1/2}$ requires more care because normalisation by the (changing) degree matrix does not preserve the Löwner order; we leave this extension to future work.

3.4.2 Direction 2: Effective Resistance and Long-Range Information Flow

Corollary 5 (Improved Scaled Kirchhoff Index). *Inspired from LASER [3], define $\mathcal{K}(\mathbf{W}_t) \triangleq \sum_{k=2}^N 1/\lambda_k(\mathbf{L}_t)$. Then*

$$\mathcal{K}(\mathbf{W}'_t) \leq \mathcal{K}(\mathbf{W}_t).$$

We show numerically that our reweighting leads to improved scaled Kirchhoff index in Table 1.

3.4.3 Direction 3: Local Bottleneck Alleviation

Definition 6 (Cut Conductance). Inspired from LASER [3], for a nonempty proper subset $S \subset \mathcal{V}$, define [3]:

$$\phi_{\mathbf{W}_t}(S) = \frac{\text{cut}(S; \mathbf{W}_t)}{\min\{\text{vol}(S; \mathbf{W}_t), \text{vol}(\mathcal{V} \setminus S; \mathbf{W}_t)\}},$$

where

$$\text{cut}(S; \mathbf{W}_t) = \sum_{i \in S, j \notin S} w_{ij,t}, \quad \text{vol}(S; \mathbf{W}_t) = \sum_{i \in S} \sum_j w_{ij,t}.$$

The Cheeger constant is defined as:

$$h(\mathcal{G}_t) = \min_{\emptyset \neq S \subsetneq \mathcal{V}} \phi_{\mathbf{W}_t}(S).$$

Proposition 7 (Local Bottleneck Alleviation). *Inspired from LASER [3], let $S \subset \mathcal{V}$ be a nontrivial cut. Assume the rewiring changes only edges crossing the boundary ∂S , i.e.*

$$w'_{ij,t} \geq w_{ij,t} \text{ for } i \in S, j \notin S, \quad w'_{ij,t} = w_{ij,t} \text{ otherwise.}$$

Then $\phi_{\mathbf{W}'_t}(S) \geq \phi_{\mathbf{W}_t}(S)$, with strict inequality if at least one crossing edge is strengthened. Therefore, if S is a curvature-identified bottleneck cut, the rewiring locally alleviates that bottleneck.

We numerically show that our reweighting method improves the local bottleneck conductance in Table 1.

Remark 8 (Scope of Local Bottleneck alleviation). The statement $\phi_{\mathbf{W}'_t}(S) \geq \phi_{\mathbf{W}_t}(S)$ holds true for any cut S , $S \subsetneq \mathcal{V}$, $S \neq \emptyset$. Proposition 7 is a graph-theoretic statement that is needed for oversquashing: negatively curved edges indicate bottlenecks, and strengthening the crossing edges of such a bottleneck increases its conductance. We note that proposition 7 does not claim global optimality; finding the set S that provides a global optimum is not guaranteed by this proposition. Numerical results illustrating $\phi_{\mathbf{W}'_t}(S)$ and $\phi_{\mathbf{W}_t}(S)$ for various S is given in the experimental section.

3.4.4 Direction 4: Probabilistic Calibration and Marginal CRPS

We evaluate our model performance using the Continuous Ranked Probability Score (CRPS) metric, defined as: $\text{CRPS}(F, y) = \mathbb{E}||X - y|| + \frac{1}{2}\mathbb{E}||X - X'||$ where $F(x)$ is the cumulative distribution function (CDF) of the forecasted distribution, y is the observed value, X, X' are sampled from F . Let CRPS_{sum} be the average sum of all marginal CRPS values computed per variate. We use CRPS_{sum} to compare the performance of the proposed method against the state of the art.

3.5 Inference-Time Residual Refinement

This section details the sampling performed by the proposed method at inference time. Direct autoregressive rollout under the batch Gaussian model may underestimate volatility or propagate early-step errors. To mitigate this, we introduce a refinement step that draws next-step residual samples from the Gaussian conditional induced by the model covariance over the window $\boldsymbol{\eta}_{t-D+2:t+1}$.

Block Partition. At forecast time $t + 1$, we follow the sampling from the gaussian posterior same as TCVAR[29]. Our sampled forecast take the spatial error propagation into account.

Node-Wise Volatility Scaling. The limitation of TCVAR is that it does not capture local volatilities. To overcome this limitation, we propose node-wise volatility scaling. Conditional covariance $\Sigma_{\text{cond},t+1}$ in Eq. (9) already contains both marginal uncertainty and spatial dependence in the original data units. Therefore, directly multiplying a Cholesky factor of $\Sigma_{\text{cond},t+1}$ by an additional empirical volatility scale may double-count marginal variance. To avoid this, we separate the conditional covariance into node-wise marginal scales and a dimensionless conditional correlation matrix. Let

$$S_{\text{cond},t+1} = \text{diag} \left(\sqrt{(\Sigma_{\text{cond},t+1})_{11}}, \dots, \sqrt{(\Sigma_{\text{cond},t+1})_{NN}} \right),$$

and define the corresponding conditional correlation matrix

$$R_{\text{cond},t+1} = S_{\text{cond},t+1}^{-1} \Sigma_{\text{cond},t+1} S_{\text{cond},t+1}^{-1}.$$

Here, $R_{\text{cond},t+1}$ is dimensionless and captures the spatial dependence structure of the conditional residual distribution.

To adapt the marginal scale to recent local volatility, we maintain for each node i an exponential moving average of squared one-step residuals. Let

$$r_{i,t} = x_{i,t} - \mu_{i,t},$$

and define

$$s_{i,t}^2 = \rho s_{i,t-1}^2 + (1 - \rho) r_{i,t}^2, \quad \rho \in [0, 1].$$

Thus, $s_{i,t}^2$ is an empirical estimate of the recent residual variance at node i , not a log-variance. We collect these estimates in the diagonal matrix

$$D_t = \text{diag}(s_{1,t}^2, \dots, s_{N,t}^2).$$

Let $R_{\text{cond},t+1}^{1/2}$ denote any matrix square root satisfying

$$R_{\text{cond},t+1}^{1/2} \left(R_{\text{cond},t+1}^{1/2} \right)^\top = R_{\text{cond},t+1}.$$

The volatility-adapted refined residual sample is then given by

$$\tilde{\eta}_{t+1}^{\text{ref}} = \mu_{\text{cond},t+1} + D_t^{1/2} R_{\text{cond},t+1}^{1/2} \xi_{t+1}, \quad \xi_{t+1} \sim \mathcal{N}(0, I_N). \quad (10)$$

This construction preserves the spatial correlation structure learned by the conditional covariance while replacing its marginal scale with a recent node-wise volatility estimate.

Training Objective. All parameters are optimized jointly by minimizing the negative log-likelihood (NLL) under the batch Gaussian model:

$$\mathcal{L} = -\log p(\boldsymbol{\eta}_t^{\text{bat}}) = \frac{DN}{2} \log(2\pi) + \frac{1}{2} \log |\Sigma_t^{\text{bat}}| + \frac{1}{2} (\boldsymbol{\eta}_t^{\text{bat}})^\top (\Sigma_t^{\text{bat}})^{-1} \boldsymbol{\eta}_t^{\text{bat}}. \quad (5)$$

Tractable evaluation exploits the Woodbury identity applied to the Kronecker structure, reducing the dominant inversion cost from $\mathcal{O}((DN)^3)$ to $\mathcal{O}(D^3 + R^3 + DNR^2)$.

4 Experiments

To demonstrate the applicability of our method, Section 4.1 introduces the dataset and the baselines used for comparison. Sections 4.2 and 4.3 describe the graph construction of our approach and present the comparative results. Sections 4.4 and 4.5 further examine model interpretability and report the results of an ablation study.

4.1 Datasets and Baselines

To assess its robustness across different scenarios, we test Teger on four real-world traffic datasets described in Table 5, and 4 backbones with diagonal Gaussian likelihoods. Specifically, the 4 backbones are the (i) Long Short-Term Memory networks [19] (LSTM) with diagonal Gaussian likelihood, serving as a fundamental sequential modeling baseline.; (ii) the standard transformer [23] architecture adapted for time series forecasting with point-wise attention and probabilistic output layers; (iii) the **xLSTM** [4], an evolution of the traditional LSTM designed to overcome its limitations in scaling and memory capacity; and (iv) the **MTGNN**[26], alternating use of graph convolution and temporal convolution modules. We include this baseline to address the possibility that gains may come from injecting spatial structure rather than from the proposed curvature-aware covariance mechanism. We compare Teger against a naive approach, which refers to raw predictions from the backbone without any temporal correlation modeling; and TCVAR [29] which models temporal error correlations but not spatial ones. Additionally, we compare Teger with a state-of-the-art rewiring method, LASER [3], which inserts edges via a sequence of augmented snapshots. A chronological 70/10/20% split is applied to all datasets. The graph construction is detailed in Appendix J.

4.2 Results

Table 1 presents CRPS_{sum} results. Teger consistently outperforms baselines, TCVAR [29], and LASER [3] across most forecasting horizons, with Teger achieving the best results in most settings. The full results with STDs are reported in Table 7. To demonstrate the effectiveness of our model, from Fig. 3 we can conclude that it is feasible to reduce prediction error in autoregressive models across future horizons by properly modeling spatial error propagation. Quantitatively, after modeling spatial error propagation and refining the forecasts, we improve the prediction quality of the TCVAR [29] model by reducing nearly 30% of the MAE error magnitude. The hyperparameters, runtime, and memory analysis are detailed in Appendix G.

Table 1: CRPS_{sum}↓ results across 4 datasets. Best result per row in **bold**.

Dataset	Backbone	15 min (3-step)				30 min (6-step)				60 min (12-step)			
		naïve	TCVAR	LASER	Teger	naïve	TCVAR	LASER	Teger	naïve	TCVAR	LASER	Teger
PeMS03	LSTM	0.0475	0.0405	0.0387	0.0383	0.0476	0.0419	0.0397	0.0401	0.0503	0.0491	0.0436	0.0401
	Transformer	0.0457	0.0355	0.0313	0.0292	0.0473	0.0371	0.0329	0.0305	0.0490	0.0386	0.0340	0.0316
	xLSTM	0.0448	0.0390	0.0351	0.0316	0.0464	0.0405	0.0360	0.0328	0.0479	0.0420	0.0377	0.0341
	MTGNN	0.0539	0.0491	0.0449	0.0428	0.0509	0.0422	0.0403	0.0445	0.0583	0.0541	0.0496	0.0483
PeMS04	LSTM	0.0229	0.0197	0.0165	0.0134	0.0242	0.0210	0.0173	0.0144	0.0255	0.0221	0.0184	0.0152
	Transformer	0.0218	0.0156	0.0136	0.0115	0.0231	0.0171	0.0150	0.0125	0.0243	0.0178	0.0156	0.0133
	xLSTM	0.0168	0.0155	0.0135	0.0112	0.0180	0.0166	0.0140	0.0120	0.0191	0.0177	0.0149	0.0128
	MTGNN	0.0301	0.0255	0.0182	0.0142	0.0335	0.0301	0.0220	0.0190	0.0310	0.0275	0.0258	0.0184
PeMS07	LSTM	0.0968	0.0956	0.0896	0.0871	0.0972	0.0949	0.0940	0.0886	0.1001	0.0989	0.0958	0.0922
	Transformer	0.0957	0.0932	0.0914	0.0871	0.0974	0.0949	0.0926	0.0886	0.0991	0.0966	0.0946	0.0901
	xLSTM	0.0941	0.0907	0.0903	0.0864	0.0958	0.0922	0.0916	0.0878	0.0975	0.0938	0.0936	0.0891
	MTGNN	0.1052	0.1013	0.0921	0.0874	0.1012	0.0955	0.1013	0.0978	0.1098	0.1023	0.1026	0.0964
Brussels	LSTM	0.1455	0.0863	0.0871	0.0809	0.1487	0.0894	0.0895	0.0811	0.1512	0.0917	0.0921	0.0842
	Transformer	0.1668	0.0786	0.0779	0.0668	0.1671	0.0793	0.0794	0.0692	0.1717	0.0817	0.0821	0.0695
	xLSTM	0.1448	0.0748	0.0752	0.0591	0.1473	0.0801	0.0828	0.0611	0.1496	0.0819	0.0821	0.0619
	MTGNN	0.1471	0.0918	0.0953	0.0853	0.1507	0.0987	0.0967	0.0832	0.1535	0.0971	0.0970	0.0935

Table 2: Comparison of graph measures before and after Algorithm 1 (in %).

Dataset	Backbone	$\mathcal{K}(W_t)/\mathcal{K}(W_t^*)$	$\lambda_{n-1}/\lambda_{n-1}^*$	$\phi_{W_t}(S)/\phi_{W_t^*}(S)$
Brussels	LSTM	34.1	37.1	33.9
	Transformer	32.4	36.3	33.6
	xLSTM	30.6	34.2	32.5
	MTGNN	20.1	23.3	29.8
PeMS04	LSTM	22.6	23.6	22.9
	Transformer	19.1	18.8	17.6
	xLSTM	17.3	15.1	14.2
	MTGNN	13.4	14.3	13.8
PeMS07	LSTM	9.1	9.3	8.9
	Transformer	8.9	8.3	7.9
	xLSTM	7.1	6.9	6.6
	MTGNN	6.8	6.3	6.8
PeMS03	LSTM	20.6	21.2	21.9
	Transformer	20.1	19.3	20.7
	xLSTM	18.6	16.5	17.1
	MTGNN	15.3	15.6	15.9

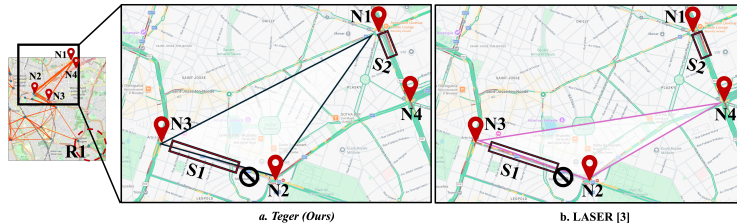


Figure 2: Analysis of a rewired subgraph in a congested area of Brussels under a sampled inference via (a.) our model (Teger) and (b.) LASER [3], illustrating the physical consistency of the curvature-based graph rewiring of our model (Teger) compared to LASER [3]. Red segments indicate congested roads, and stop signs denote partial road closures. Data source: Google Maps.

4.3 Model Interpretability

Quantitative experiments across 48 (dataset, backbone, horizon) configurations in Table 1 show that Teger achieves the best CRPS in 42 cases. LASER outperforms Teger primarily on PeMS03 at longer horizons. Notably, the gap is largest on the Brussels dataset (Teger improves CRPS by 25.3% over LASER [3]), where the road network is densest and the most physically constrained. Figure 2 illustrates why this gap appears on road graphs specifically: LASER’s added edges (e.g., N3–N4) do not correspond to physically realized routes, introducing covariance pathways that are not mediated by the underlying transportation infrastructure. Teger’s reweighting preserves the correspondence between graph topology and physical road structure, which we hypothesize accounts for the quantitative advantage on dense urban networks.

Use Case: Teger’s interpretability in Brussels dataset. This section provides a qualitative illustration of the curvature-aware rewiring mechanism applied to the Brussels traffic sensor network under the xLSTM backbone (Teger). The goal is to examine whether the edges that receive the strongest covariance amplification are geographically consistent with locations that plausibly exhibit correlated sensor errors. This subsection constitutes a visualization exercise, not a quantitative validation against independent ground-truth bottleneck labels; a rigorous validation against incident

Table 3: Ablation study on curvature-aware spatial correlation variants.

Variant	NLL \downarrow	MAE \downarrow
No rewiring	72.21	8.21
- Volatility Modeling	66.21	7.01
+ Edge reweighting	58.21	5.91
+ Latent projection (full)	49.32	4.98

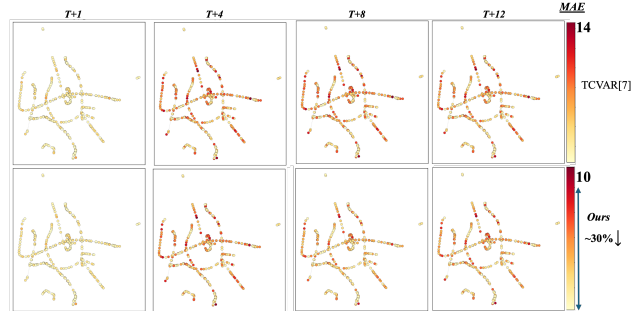


Figure 3: Analysis of spatial error propagation reduction for PeMS03 dataset. The top row shows the forecasts from the TCVAR [29] method, while the bottom row shows the results from Teger.

logs, empirical residual cross-correlations, or measured queue spillback data is left for future work. We have a similar observations in the cities with different topologies. Network description is detailed in Appendix I. Similar observations as above have been made on cities with different graph topologies.

Physical interpretation and limitations. The curvature mechanism selectively amplifies covariance coupling along sensor pairs that are in close proximity but share few common alternative sensor neighbours — a structural signature consistent with corridor-like sensor placements on long arterial segments. For such pairs, a disruption at one sensor (due to congestion, an incident, or roadworks) is more likely to produce statistically co-varying forecast residuals at the neighbouring sensor, because both observe the same traffic stream with little spatial diversification. The term *rewired* denotes that the model has increased the covariance between those sensors; it does not imply causal traffic propagation, which would require independent validation against speed measurements or incident records.

Ablation Study. As reported in Table 3, curvature-aware rewiring consistently improves over the standard graph formulation. These numerical results were obtained on PeMS378 data; similar findings are obtained on other datasets. Edge reweighting based on negative curvature alleviates information bottlenecks, leading to better long-range dependency modeling. The full formulation, including latent-space projection and precision matrix construction, yields the best performance, highlighting the importance of combining geometric insights with low-rank modelling.

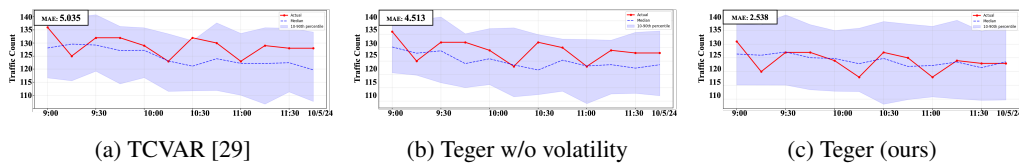


Figure 4: Qualitative comparison of results forecasted by baseline and variants of Teger for the Brussels dataset, annotated by the corresponding MAE.

5 Conclusion

We presented Teger, a probabilistic framework for multivariate time-series forecasting that explicitly models spatially correlated forecast errors via graph-structured covariances. We proposed a spatial component: a curvature-aware rewiring mechanism.

References

- [1] Uri Alon and Eran Yahav. On the bottleneck of graph neural networks and its practical implications. In *9th International Conference on Learning Representations, ICLR 2021*, 2021.
- [2] Arjun Ashok, Étienne Marcotte, Valentina Zantedeschi, Nicolas Chapados, and Alexandre Drouin. Tactis-2: Better, faster, simpler attentional copulas for multivariate time series, 2024.
- [3] Federico Barbero, Ameya Velingker, Amin Saberi, Michael M. Bronstein, and Francesco Di Giovanni. Locality-aware graph rewiring in GNNs. In *The Twelfth International Conference on Learning Representations*, 2024.
- [4] Maximilian Beck, Korbinian Poppel, Markus Spanring, Andreas Auer, Oleksandra Prudnikova, Michael Kopp, Gunter Klambauer, Johannes Brandstetter, and Sepp Hochreiter. xlstm: Extended long short-term memory. *Advances in Neural Information Processing Systems*, 37:107547–107603, 2024.
- [5] Konstantinos Benidis, Syama Sundar Rangapuram, Valentin Flunkert, Yuyang Wang, Danielle Maddix, Caner Turkmen, Jan Gasthaus, Michael Bohlke-Schneider, David Salinas, Lorenzo Stella, François-Xavier Aubet, Laurent Callot, and Tim Januschowski. Deep learning for time series forecasting: Tutorial and literature survey. *ACM Computing Surveys*, 55(6):1–36, December 2022.
- [6] Nicholas J. Higham. *Accuracy and stability of numerical algorithms*. Society for Industrial and Applied Mathematics (SIAM), Philadelphia, PA, second edition, 2002.
- [7] Roger A. Horn and Charles R. Johnson. *Matrix Analysis*. Cambridge University Press, 1985.
- [8] Shiyang Li, Xiaoyong Jin, Yao Xuan, Xiyong Zhou, Wenhui Chen, Yu-Xiang Wang, and Xifeng Yan. Enhancing the locality and breaking the memory bottleneck of transformer on time series forecasting, 2020.
- [9] Weijun Li, Guoliang Yang, Zhangyou Xiong, Xiaojuan Zhu, and Xinyu Ma. A traffic flow prediction model based on dynamic graph convolution and adaptive spatial feature extraction. *Symmetry*, 17(7), 2025.
- [10] Yaguang Li, Rose Yu, Cyrus Shahabi, and Yan Liu. Diffusion convolutional recurrent neural network: Data-driven traffic forecasting. In *International Conference on Learning Representations*, 2018.
- [11] Bryan Lim, Sercan O. Arik, Nicolas Loeff, and Tomas Pfister. Temporal fusion transformers for interpretable multi-horizon time series forecasting, 2020.
- [12] Shizhan Liu, Hang Yu, Cong Liao, Jianguo Li, Weiyao Lin, Alex X. Liu, and Schahram Dustdar. Pyraformer: Low-complexity pyramidal attention for long-range time series modeling and forecasting. In *International Conference on Learning Representations*, 2022.
- [13] Ivan Marisca, Jacob Bamberger, Cesare Alippi, and Michael M Bronstein. Over-squashing in spatiotemporal graph neural networks. In *The Thirty-ninth Annual Conference on Neural Information Processing Systems*.
- [14] Seyed Mohamad Moghadas, Amin Gheibi, and Alexander Alahi. Statnet: Spatial-temporal attention in the traffic prediction. In *hEART 2022: 10th Symposium of the European Association for Research in Transportation*, 2022.
- [15] Zelin Ni, Hang Yu, Shizhan Liu, Jianguo Li, and Weiyao Lin. Basisformer: Attention-based time series forecasting with learnable and interpretable basis, 2024.
- [16] Yuqi Nie, Nam H. Nguyen, Phanwadee Sinthong, and Jayant Kalagnanam. A time series is worth 64 words: Long-term forecasting with transformers, 2023.
- [17] Boris N. Oreshkin, Dmitri Carпов, Nicolas Chapados, and Yoshua Bengio. N-beats: Neural basis expansion analysis for interpretable time series forecasting, 2020.

- [18] Weizhu Qian, Yan Zhao, Dalin Zhang, Bowei Chen, Kai Zheng, and Xiaofang Zhou. Towards a unified understanding of uncertainty quantification in traffic flow forecasting, 01 2023.
- [19] David Salinas, Michael Bohlke-Schneider, Laurent Callot, Roberto Medico, and Jan Gasthaus. High-dimensional multivariate forecasting with low-rank gaussian copula processes, 2019.
- [20] Chao Shang, Jie Chen, and Jinbo Bi. Discrete graph structure learning for forecasting multiple time series. In *International Conference on Learning Representations*, 2021.
- [21] Chao Song, Youfang Lin, Shengnan Guo, and Huaiyu Wan. Spatial-temporal synchronous graph convolutional networks: A new framework for spatial-temporal network data forecasting. *Proceedings of the AAAI Conference on Artificial Intelligence*, 34(01):914–921, Apr. 2020.
- [22] Jake Topping, Francesco Di Giovanni, Benjamin Paul Chamberlain, Xiaowen Dong, and Michael M. Bronstein. Understanding over-squashing and bottlenecks on graphs via curvature, 2022.
- [23] Ashish Vaswani, Noam Shazeer, Niki Parmar, Jakob Uszkoreit, Llion Jones, Aidan N. Gomez, Lukasz Kaiser, and Illia Polosukhin. Attention is all you need, 2023.
- [24] Gerald Woo, Chenghao Liu, Doyen Sahoo, Akshat Kumar, and Steven Hoi. Etsformer: Exponential smoothing transformers for time-series forecasting, 2022.
- [25] Haixu Wu, Jiehui Xu, Jianmin Wang, and Mingsheng Long. Autoformer: Decomposition transformers with auto-correlation for long-term series forecasting, 2022.
- [26] Zonghan Wu, Shirui Pan, Guodong Long, Jing Jiang, Xiaojun Chang, and Chengqi Zhang. Connecting the dots: Multivariate time series forecasting with graph neural networks. In *Proceedings of the 26th ACM SIGKDD International Conference on Knowledge Discovery & Data Mining*, KDD ’20, page 753–763, New York, NY, USA, 2020. Association for Computing Machinery.
- [27] Zonghan Wu, Shirui Pan, Guodong Long, Jing Jiang, and Chengqi Zhang. Graph wavenet for deep spatial-temporal graph modeling. In *Proceedings of the Twenty-Eighth International Joint Conference on Artificial Intelligence, IJCAI-19*, pages 1907–1913. International Joint Conferences on Artificial Intelligence Organization, 7 2019.
- [28] Chuanpan Zheng, Xiaoliang Fan, Cheng Wang, and Jianzhong Qi. Gman: A graph multi-attention network for traffic prediction. *Proceedings of the AAAI Conference on Artificial Intelligence*, 34(01):1234–1241, Apr. 2020.
- [29] Vincent Zhihao Zheng and Lijun Sun. Multivariate probabilistic time series forecasting with correlated errors. In *The Thirty-eighth Annual Conference on Neural Information Processing Systems*, 2024.
- [30] Haoyi Zhou, Shanghang Zhang, Jieqi Peng, Shuai Zhang, Jianxin Li, Hui Xiong, and Wancai Zhang. Informer: Beyond efficient transformer for long sequence time-series forecasting, 2021.
- [31] Tian Zhou, Ziqing Ma, Qingsong Wen, Xue Wang, Liang Sun, and Rong Jin. Fedformer: Frequency enhanced decomposed transformer for long-term series forecasting, 2022.

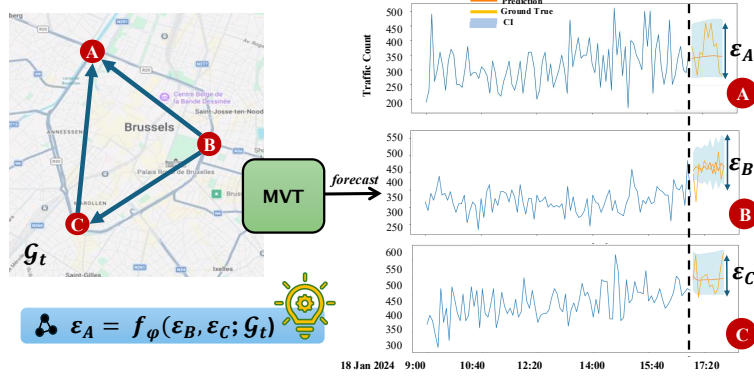
A Motivation

B Proofs

B.1 Proof of Proposition 1 (Validity of Rewired Covariance)

Part (i). The graph Laplacian of any symmetric, entrywise nonnegative matrix is PSD: $\mathbf{x}^\top \mathbf{L}'_t \mathbf{x} = \frac{1}{2} \sum_{i,j} W'_{ij,t} (x_i - x_j)^2 \geq 0$ for all $\mathbf{x} \in \mathbb{R}^N$.

Part (ii). For any $\mathbf{x} \in \mathbb{R}^R$, $\mathbf{x}^\top \mathbf{L}'_t^{(R)} \mathbf{x} = (\mathbf{P}\mathbf{x})^\top \mathbf{L}'_t (\mathbf{P}\mathbf{x}) \geq 0$ since $\mathbf{L}'_t \succeq \mathbf{0}$ by Part (i).



(a) Motivation for modeling spatial error propagation in traffic forecasting. A multivariate time series (MVT) model generates traffic forecasts for multiple traffic cameras located on the intricate road network of Brussels, Belgium. Our model is designed to explicitly capture and refine predictions by accounting for correlated forecast uncertainties across the transportation network based on their spatial dependency.

(b) Empirical spatio-temporal covariance on the PeMS03 dataset is estimated from LSTM residuals of traffic speed forecasts. The results exhibit both contemporaneous spatial structure and cross-lag temporal persistence in the residuals, motivating the joint spatio-temporal covariance model introduced in Section 3.3.1.

Figure 5: Motivation of our work.

Part (iii). For any $\mathbf{x} \neq \mathbf{0}$, $\mathbf{x}^\top \mathbf{Q}_t \mathbf{x} = \alpha \|\mathbf{x}\|^2 + \beta \mathbf{x}^\top \mathbf{L}_t^{(R)} \mathbf{x} + \sigma_{\min} \|\mathbf{x}\|^2 \geq (\alpha + \sigma_{\min}) \|\mathbf{x}\|^2 > 0$, so $\mathbf{Q}_t \succ \mathbf{0}$ and hence $\mathbf{G}_t = \mathbf{Q}_t^{-1}$ is symmetric positive definite. \square

B.2 Proof of Lemma 2 (Laplacian Monotonicity)

Proof. For any symmetric non-negative weight matrix \mathbf{A} , the unnormalised Laplacian is $\mathbf{L}_\mathbf{A} = \text{diag}(\mathbf{A}) - \mathbf{A} \triangleq \mathbf{D} - \mathbf{A}$ where \mathbf{D} is the degree matrix. Linearity of Lemma 2 gives $\mathbf{L}_{\mathbf{W} + \Delta \mathbf{W}} = \mathbf{L}_\mathbf{W} + \mathbf{L}_{\Delta \mathbf{W}}$. The standard quadratic-form identity yields $\mathbf{x}^\top \mathbf{L}_{\Delta \mathbf{W}} \mathbf{x} = \frac{1}{2} \sum_{i,j} \Delta w_{ij} (x_i - x_j)^2 \geq 0$ for all \mathbf{x} , so $\mathbf{L}_{\Delta \mathbf{W}} \succeq \mathbf{0}$. \square

B.3 Proof of Proposition 3 (Spectral Gap Monotonicity)

Proof. Write $\Delta \mathbf{W}_t = \mathbf{W}'_t - \mathbf{W}_t$. By the rewiring rule,

$$W'_{i,j,t} = W_{i,j,t}(1 + \lambda b_{i,j,t}), \quad \lambda > 0, \quad b_{i,j,t} \geq 0,$$

so $\Delta \mathbf{W}_t \geq 0$ entrywise. By Lemma 2,

$$\mathbf{L}'_t = \mathbf{L}_t + \mathbf{L}_{\Delta \mathbf{W}_t}, \quad \mathbf{L}_{\Delta \mathbf{W}_t} \succeq \mathbf{0},$$

which proves (i).

For (ii), since it is a classical algebraic statement, the reader can see Corollary 4.3.12[7]. \square

B.4 Proof of Corollary 5

(Improved Scaled Kirchhoff Index).

Proof. Since

$$\mathbf{L}'_t = \mathbf{L}_t + \mathbf{L}_{\Delta}\mathbf{w}_t, \quad \mathbf{L}_{\Delta}\mathbf{w}_t \succeq 0,$$

According to Corollary 4.3.12[7], the following holds:

$$\lambda_k(\mathbf{L}'_t) \geq \lambda_k(\mathbf{L}_t) \quad (k = 1, \dots, N).$$

Therefore

$$\mathcal{K}(\mathbf{W}'_t) = \sum_{k=2}^N 1/\lambda_k(\mathbf{L}'_t) \leq \sum_{k=2}^N 1/\lambda_k(\mathbf{L}_t) = \mathcal{K}(\mathbf{W}_t).$$

□

B.5 Proof of Proposition 7

Proof. The proof is given in LASER [3].

□

C Notation Table

Table 4: Summary of key notation used in Section 3.

Symbol	Definition
$\mathcal{G}_t = (\mathcal{V}, \mathcal{E}_t, \mathbf{A}_t)$	Dynamic graph (topology only)
$\mathbf{A}_t \in \mathbb{R}^{N \times N}$	Adjacency matrix of \mathcal{G}_t
$\mathbf{L}'_t \in \mathbb{R}^{N \times N}$	Rewired graph Laplacian (Algorithm 1)
$\Sigma_t^{\text{spa}} \in \mathbb{R}^{R \times R}$	Spatial factor covariance
$\mathbf{C}_t \in \mathbb{R}^{D \times D}$	Temporal kernel-mixture correlation matrix
$\mathbf{\Pi} \in \mathbb{R}^{N \times R}$	Learnable projection matrix ($\mathbf{P} = \text{colnorm}(\mathbf{\Pi})$)
$\Gamma_t \in \mathbb{R}^{N \times N}$	Cholesky factor of conditional covariance
$\boldsymbol{\eta}_t^{\text{bat}} \in \mathbb{R}^{DN}$	Stacked residuals $\text{vec}(\boldsymbol{\eta}_{t-D+1:t})$
$\Sigma_t^{\text{bat}} \in \mathbb{R}^{DN \times DN}$	Batch covariance over window D
$\mathbf{D}_t \in \mathbb{R}^{N \times N}$	Diagonal node-wise volatility scaling
$\kappa_{ij,t}$	Balanced Forman curvature of edge (i, j) at time t
$b_{ij,t}$	Bottleneck score = $\text{softplus}(\tau(\kappa_0 - \kappa_{ij,t}))$
$h(\mathcal{G})$	Cheeger (edge expansion) constant of graph \mathcal{G}
$R_{\text{eff}}(i, j)$	Effective resistance between nodes i and j
$\mathcal{K}(\mathbf{W})$	Kirchhoff index (total effective resistance)

D Implementation Details

All models in the paper were trained in a Conda environment running on an Intel 13900F and 2 NVIDIA RTX 4090 with 24 GB. Our Pytorch version is 1.13.1 with CUDA 11.7.

E Datasets Description

Table 5: Datasets Description.

Dataset	Data Type	Region	Nodes	Time Steps
PeMS03	Traffic Speed	California	358	26208
PeMS04	Traffic Speed	California	307	16992
PeMS07	Traffic Speed	California	883	26208
Brussels	Traffic Count	Brussels	195	12672

F Memory and Runtime

We evaluate the performance of our proposed method compared to TCVAR and LASER in terms of memory and runtime computation resources, which the results are shown in Figure 6.

Brussels Dataset: Runtime and Memory Comparison

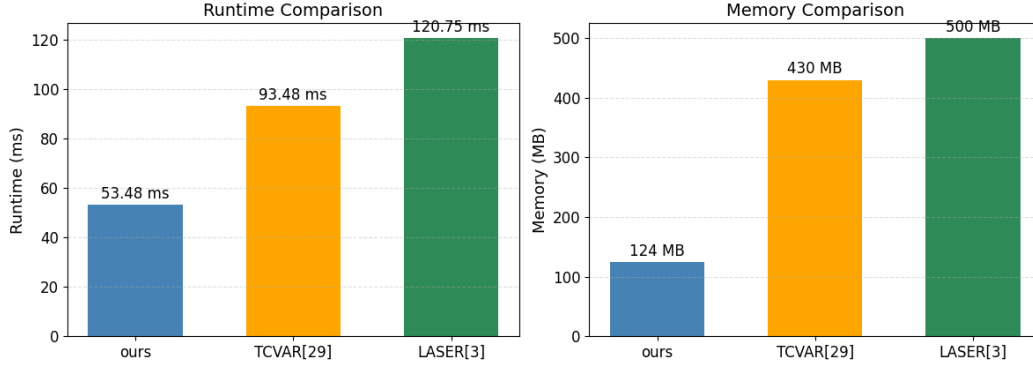


Figure 6: Analysis of computation resources for Brussels dataset. Teger consumes resources less than TCVAR [29] and LASER [3] methods, while forecasting more accurately.

Table 6: Hyperparameter settings.

Group	Parameter	Value
Training	Max epochs	100
	Max steps	10,000
	Node batch size B	20
	Gradient clip	10.0
	Weight decay	10^{-8}
Backbone	Hidden dim H	40
	RNN/xLSTM/Transformers layers	2
	Dropout	0.01
Temporal Correlation	Batch horizon D	12
	Mixture components M	4
	Low-rank dim R	10
	Length-scale step σ'	1.0
	Loss LR / weight decay	$10^{-3} / 10^{-8}$
Curvature (Alg. 1)	Precision diag. α	0.01
	Laplacian weight β	1.0
	Bottleneck strength λ	1.0
	Curvature threshold κ_0	0.0
	Sensitivity τ	5.0
	Proj. floor σ_{\min}	10^{-4}
Optimization	Learning Rate η	$\{10^{-3}, 10^{-2}\}$

G Hyperparameter Tuning

The hyperparameter search span and the optimal choice are summarized in Table 6.

H Statistical Significance Test

The statistical significance test is detailed in Table 7.

I Brussels Reweighting Details

The Brussels graph contains 6,632 undirected edges. Balanced Forman curvature values lie in the range $[-0.2025, +0.4151]$ with mean $\bar{\kappa} = -0.0755$ and standard deviation $\sigma_{\kappa} = 0.0565$. As expected for a proximity-based sensor graph, 95.4% of edges have $\kappa_{ij} < 0$: most sensor pairs lie along chain-like corridors without shared alternative sensor neighbors, which produces negative Balanced

Table 7: Teger statistical significance over 24 rolling forecast test windows. Values are mean \pm std across windows. QL0.5, and QL0.9 use the aggregate values reported in the existing metrics files.

Backbone	Dataset	CRPS-mean	CRPS-sum	QL0.5	QL0.9
xLSTM	Brussels	0.0239 \pm 0.0002	0.0619 \pm 0.0094	0.0141 \pm 0.0001	0.0096 \pm 0.0001
	pems03	0.0270 \pm 0.0019	0.0341 \pm 0.0023	0.0210 \pm 0.0001	0.0362 \pm 0.0001
Transformer	Brussels	0.0275 \pm 0.0099	0.0695 \pm 0.0108	0.0161 \pm 0.0001	0.0111 \pm 0.0001
	pems03	0.0311 \pm 0.0022	0.0316 \pm 0.0026	0.0242 \pm 0.0001	0.0416 \pm 0.0002



Figure 7: An illustrative traffic snapshot at the three annotated sensor clusters. Images are static snapshots from Google Map service and were not selected to match any specific traffic event in the dataset.

Forman curvature by construction. Of the 6632 edges, the model designates 663 (10%) as *rewired*, defined as those whose bottleneck score b_{ij} meets or exceeds the 90th percentile of the full edge distribution ($b \geq 2.20$); the remaining 90% receive negligible reweighting ($W'_{ij}/W_{ij} \approx 1$). We annotate three sensor clusters in Figure 2, chosen to span the range of bottleneck behavior. Node N1 corresponds to the sensor (Schaerbeek municipality), which has the highest mean incident bottleneck score of any sensor in the network ($\bar{b}=3.70$). Its five strongest edges all connect to neighbouring Schaerbeek sensors and achieve Balanced Forman curvature in the range $[-0.198, -0.203]$, more than two standard deviations below the graph mean, resulting in covariance reweighting of $10.9\text{--}11.3\times$ (Table 8, row E1). These sensor pairs share only 74–82 common sensor neighbors despite each node having degree 85–108. Node N2 (0.7 km from Place Robert Schuman, $\bar{\kappa}=-0.078$). Its strongest rewired edge connects to Etterbeek sensor N2 with $\kappa=-0.121$, $W'/W=4.43\times$, and 63 common neighbours (Table 8, row E2). Node N3 (approximately 0.6 km from Arts-Loi junction), whose strongest rewired edge to the same Etterbeek sensor yields $\kappa=-0.110$ and $W'/W=3.52\times$ (row E3). Cross-municipality edges (Brussels \leftrightarrow Etterbeek) appear prominently among rewired edges because the two sensor clusters share proportionally fewer common neighbours than intra-municipality pairs, lowering κ and raising b . For comparison, row R1 shows a representative non-rewired edge in the Auderghem sub-cluster: $\kappa=+0.415$, $|\Delta|=10$ (proportionally high relative to node degree), and $W'/W=1.00$ — the model correctly assigns zero amplification to this geometrically well-connected pair.

The street imagery in Figure 7 provides geographic context for clusters N1–N3 and is presented as illustrative background only. It was not used as evidence for model correctness and cannot be independently reproduced as quantitative validation. The graph’s Euclidean-distance construction means that the edges highlighted here reflect sensor-proximity bottlenecks; claims about specific road-network features (tunnels, ring roads) cannot be formally substantiated without a topology-derived graph, and we do not make such claims here.

J Graph construction

For PeMS and Brussels datasets, the adjacency matrix A is the thresholded Gaussian kernel $A_{ij} = \exp(-d_{ij}^2/(2\sigma^2))$ if $A_{ij} \geq 0.1$, else 0, where d_{ij} is the road network distance between sensors i and j and σ is the standard deviation of all pairwise distances. For Brussels, GPS Euclidean distance is used in place of road-network distance. The resulting graphs are symmetric, connected, and held fixed across all experiments. We build the dynamic graph, consequently, as in [9]. For PeMS datasets, the dynamic graph is given.

Table 8: Brussels edge statistics.

Label	Sensor pair	κ	W	W'	W'/W	$ \Delta $	Rev.
<i>Rewired edges — strong bottleneck signal</i>							
E1	N1 \leftrightarrow N3	-0.203	0.701	7.923	11.30 \times	74	✓
E2	N1 \leftrightarrow N2	-0.121	0.689	3.055	4.43 \times	63	✓
E3	N2 \leftrightarrow N3	-0.110	0.586	2.061	3.52 \times	59	✓
<i>Non-rewired reference edge — well-connected cluster</i>							
R1	—	+0.415	1.000	1.000	1.00 \times	10	—

NeurIPS Paper Checklist

1. Claims

Question: Do the main claims made in the abstract and introduction accurately reflect the paper’s contributions and scope?

Answer: [Yes]

Justification: We clarify the contributions and the scope in the abstract and the introduction.

Guidelines:

- The answer [N/A] means that the abstract and introduction do not include the claims made in the paper.
- The abstract and/or introduction should clearly state the claims made, including the contributions made in the paper and important assumptions and limitations. A [No] or [N/A] answer to this question will not be perceived well by the reviewers.
- The claims made should match theoretical and experimental results, and reflect how much the results can be expected to generalize to other settings.
- It is fine to include aspirational goals as motivation as long as it is clear that these goals are not attained by the paper.

2. Limitations

Question: Does the paper discuss the limitations of the work performed by the authors?

Answer: [Yes]

Justification: It has been discussed in Section 4.3.

Guidelines:

- The answer [N/A] means that the paper has no limitation while the answer [No] means that the paper has limitations, but those are not discussed in the paper.
- The authors are encouraged to create a separate “Limitations” section in their paper.
- The paper should point out any strong assumptions and how robust the results are to violations of these assumptions (e.g., independence assumptions, noiseless settings, model well-specification, asymptotic approximations only holding locally). The authors should reflect on how these assumptions might be violated in practice and what the implications would be.
- The authors should reflect on the scope of the claims made, e.g., if the approach was only tested on a few datasets or with a few runs. In general, empirical results often depend on implicit assumptions, which should be articulated.
- The authors should reflect on the factors that influence the performance of the approach. For example, a facial recognition algorithm may perform poorly when image resolution is low or images are taken in low lighting. Or a speech-to-text system might not be used reliably to provide closed captions for online lectures because it fails to handle technical jargon.
- The authors should discuss the computational efficiency of the proposed algorithms and how they scale with dataset size.
- If applicable, the authors should discuss possible limitations of their approach to address problems of privacy and fairness.

- While the authors might fear that complete honesty about limitations might be used by reviewers as grounds for rejection, a worse outcome might be that reviewers discover limitations that aren't acknowledged in the paper. The authors should use their best judgment and recognize that individual actions in favor of transparency play an important role in developing norms that preserve the integrity of the community. Reviewers will be specifically instructed to not penalize honesty concerning limitations.

3. Theory assumptions and proofs

Question: For each theoretical result, does the paper provide the full set of assumptions and a complete (and correct) proof?

Answer: [Yes]

Justification: Theorems and Lemmas are presented in the main texts. Proofs are explained in the Appendix B.

Guidelines:

- The answer [N/A] means that the paper does not include theoretical results.
- All the theorems, formulas, and proofs in the paper should be numbered and cross-referenced.
- All assumptions should be clearly stated or referenced in the statement of any theorems.
- The proofs can either appear in the main paper or the supplemental material, but if they appear in the supplemental material, the authors are encouraged to provide a short proof sketch to provide intuition.
- Inversely, any informal proof provided in the core of the paper should be complemented by formal proofs provided in appendix or supplemental material.
- Theorems and Lemmas that the proof relies upon should be properly referenced.

4. Experimental result reproducibility

Question: Does the paper fully disclose all the information needed to reproduce the main experimental results of the paper to the extent that it affects the main claims and/or conclusions of the paper (regardless of whether the code and data are provided or not)?

Answer: [Yes]

Justification: We provide details in Section 4.

Guidelines:

- The answer [N/A] means that the paper does not include experiments.
- If the paper includes experiments, a [No] answer to this question will not be perceived well by the reviewers: Making the paper reproducible is important, regardless of whether the code and data are provided or not.
- If the contribution is a dataset and/or model, the authors should describe the steps taken to make their results reproducible or verifiable.
- Depending on the contribution, reproducibility can be accomplished in various ways. For example, if the contribution is a novel architecture, describing the architecture fully might suffice, or if the contribution is a specific model and empirical evaluation, it may be necessary to either make it possible for others to replicate the model with the same dataset, or provide access to the model. In general, releasing code and data is often one good way to accomplish this, but reproducibility can also be provided via detailed instructions for how to replicate the results, access to a hosted model (e.g., in the case of a large language model), releasing of a model checkpoint, or other means that are appropriate to the research performed.
- While NeurIPS does not require releasing code, the conference does require all submissions to provide some reasonable avenue for reproducibility, which may depend on the nature of the contribution. For example
 - (a) If the contribution is primarily a new algorithm, the paper should make it clear how to reproduce that algorithm.
 - (b) If the contribution is primarily a new model architecture, the paper should describe the architecture clearly and fully.

- (c) If the contribution is a new model (e.g., a large language model), then there should either be a way to access this model for reproducing the results or a way to reproduce the model (e.g., with an open-source dataset or instructions for how to construct the dataset).
- (d) We recognize that reproducibility may be tricky in some cases, in which case authors are welcome to describe the particular way they provide for reproducibility. In the case of closed-source models, it may be that access to the model is limited in some way (e.g., to registered users), but it should be possible for other researchers to have some path to reproducing or verifying the results.

5. Open access to data and code

Question: Does the paper provide open access to the data and code, with sufficient instructions to faithfully reproduce the main experimental results, as described in supplemental material?

Answer: [Yes]

Justification: We provide the data and code in supplementary materials. We are not allowed to publish the dataset for Brussels traffic because it is private. However, the scripts to reproduce the results are uploaded.

Guidelines:

- The answer [N/A] means that paper does not include experiments requiring code.
- Please see the NeurIPS code and data submission guidelines (<https://neurips.cc/public/guides/CodeSubmissionPolicy>) for more details.
- While we encourage the release of code and data, we understand that this might not be possible, so [No] is an acceptable answer. Papers cannot be rejected simply for not including code, unless this is central to the contribution (e.g., for a new open-source benchmark).
- The instructions should contain the exact command and environment needed to run to reproduce the results. See the NeurIPS code and data submission guidelines (<https://neurips.cc/public/guides/CodeSubmissionPolicy>) for more details.
- The authors should provide instructions on data access and preparation, including how to access the raw data, preprocessed data, intermediate data, and generated data, etc.
- The authors should provide scripts to reproduce all experimental results for the new proposed method and baselines. If only a subset of experiments are reproducible, they should state which ones are omitted from the script and why.
- At submission time, to preserve anonymity, the authors should release anonymized versions (if applicable).
- Providing as much information as possible in supplemental material (appended to the paper) is recommended, but including URLs to data and code is permitted.

6. Experimental setting/details

Question: Does the paper specify all the training and test details (e.g., data splits, hyperparameters, how they were chosen, type of optimizer) necessary to understand the results?

Answer: [Yes]

Justification: We provide details in Section 4.

Guidelines:

- The answer [N/A] means that the paper does not include experiments.
- The experimental setting should be presented in the core of the paper to a level of detail that is necessary to appreciate the results and make sense of them.
- The full details can be provided either with the code, in appendix, or as supplemental material.

7. Experiment statistical significance

Question: Does the paper report error bars suitably and correctly defined or other appropriate information about the statistical significance of the experiments?

Answer: [Yes]

Justification: We provide details in Section 4.

Guidelines:

- The answer [N/A] means that the paper does not include experiments.
- The authors should answer [Yes] if the results are accompanied by error bars, confidence intervals, or statistical significance tests, at least for the experiments that support the main claims of the paper.
- The factors of variability that the error bars are capturing should be clearly stated (for example, train/test split, initialization, random drawing of some parameter, or overall run with given experimental conditions).
- The method for calculating the error bars should be explained (closed form formula, call to a library function, bootstrap, etc.)
- The assumptions made should be given (e.g., Normally distributed errors).
- It should be clear whether the error bar is the standard deviation or the standard error of the mean.
- It is OK to report 1-sigma error bars, but one should state it. The authors should preferably report a 2-sigma error bar than state that they have a 96% CI, if the hypothesis of Normality of errors is not verified.
- For asymmetric distributions, the authors should be careful not to show in tables or figures symmetric error bars that would yield results that are out of range (e.g., negative error rates).
- If error bars are reported in tables or plots, the authors should explain in the text how they were calculated and reference the corresponding figures or tables in the text.

8. Experiments compute resources

Question: For each experiment, does the paper provide sufficient information on the computer resources (type of compute workers, memory, time of execution) needed to reproduce the experiments?

Answer: [Yes]

Justification: We provide details in Section 4.

Guidelines:

- The answer [N/A] means that the paper does not include experiments.
- The paper should indicate the type of compute workers CPU or GPU, internal cluster, or cloud provider, including relevant memory and storage.
- The paper should provide the amount of compute required for each of the individual experimental runs as well as estimate the total compute.
- The paper should disclose whether the full research project required more compute than the experiments reported in the paper (e.g., preliminary or failed experiments that didn't make it into the paper).

9. Code of ethics

Question: Does the research conducted in the paper conform, in every respect, with the NeurIPS Code of Ethics [https://neurips.cc/public/EthicsGuidelines?](https://neurips.cc/public/EthicsGuidelines)

Answer: [Yes]

Justification: This paper conforms, in every respect, with the NeurIPS Code of Ethics.

Guidelines:

- The answer [N/A] means that the authors have not reviewed the NeurIPS Code of Ethics.
- If the authors answer [No], they should explain the special circumstances that require a deviation from the Code of Ethics.
- The authors should make sure to preserve anonymity (e.g., if there is a special consideration due to laws or regulations in their jurisdiction).

10. Broader impacts

Question: Does the paper discuss both potential positive societal impacts and negative societal impacts of the work performed?

Answer: [N/A]

Justification: We think our work will not have a significant social impact.

Guidelines:

- The answer [N/A] means that there is no societal impact of the work performed.
- If the authors answer [N/A] or [No], they should explain why their work has no societal impact or why the paper does not address societal impact.
- Examples of negative societal impacts include potential malicious or unintended uses (e.g., disinformation, generating fake profiles, surveillance), fairness considerations (e.g., deployment of technologies that could make decisions that unfairly impact specific groups), privacy considerations, and security considerations.
- The conference expects that many papers will be foundational research and not tied to particular applications, let alone deployments. However, if there is a direct path to any negative applications, the authors should point it out. For example, it is legitimate to point out that an improvement in the quality of generative models could be used to generate Deepfakes for disinformation. On the other hand, it is not needed to point out that a generic algorithm for optimizing neural networks could enable people to train models that generate Deepfakes faster.
- The authors should consider possible harms that could arise when the technology is being used as intended and functioning correctly, harms that could arise when the technology is being used as intended but gives incorrect results, and harms following from (intentional or unintentional) misuse of the technology.
- If there are negative societal impacts, the authors could also discuss possible mitigation strategies (e.g., gated release of models, providing defenses in addition to attacks, mechanisms for monitoring misuse, mechanisms to monitor how a system learns from feedback over time, improving the efficiency and accessibility of ML).

11. Safeguards

Question: Does the paper describe safeguards that have been put in place for responsible release of data or models that have a high risk for misuse (e.g., pre-trained language models, image generators, or scraped datasets)?

Answer: [N/A]

Justification: The paper poses no such risks.

Guidelines:

- The answer [N/A] means that the paper poses no such risks.
- Released models that have a high risk for misuse or dual-use should be released with necessary safeguards to allow for controlled use of the model, for example by requiring that users adhere to usage guidelines or restrictions to access the model or implementing safety filters.
- Datasets that have been scraped from the Internet could pose safety risks. The authors should describe how they avoided releasing unsafe images.
- We recognize that providing effective safeguards is challenging, and many papers do not require this, but we encourage authors to take this into account and make a best faith effort.

12. Licenses for existing assets

Question: Are the creators or original owners of assets (e.g., code, data, models), used in the paper, properly credited and are the license and terms of use explicitly mentioned and properly respected?

Answer: [Yes]

Justification: All assets used in this paper are properly credited.

Guidelines:

- The answer [N/A] means that the paper does not use existing assets.
- The authors should cite the original paper that produced the code package or dataset.
- The authors should state which version of the asset is used and, if possible, include a URL.

- The name of the license (e.g., CC-BY 4.0) should be included for each asset.
- For scraped data from a particular source (e.g., website), the copyright and terms of service of that source should be provided.
- If assets are released, the license, copyright information, and terms of use in the package should be provided. For popular datasets, paperswithcode.com/datasets has curated licenses for some datasets. Their licensing guide can help determine the license of a dataset.
- For existing datasets that are re-packaged, both the original license and the license of the derived asset (if it has changed) should be provided.
- If this information is not available online, the authors are encouraged to reach out to the asset's creators.

13. **New assets**

Question: Are new assets introduced in the paper well documented and is the documentation provided alongside the assets?

Answer: [Yes]

Justification: We provide the documentation in the code repo.

Guidelines:

- The answer [N/A] means that the paper does not release new assets.
- Researchers should communicate the details of the dataset/code/model as part of their submissions via structured templates. This includes details about training, license, limitations, etc.
- The paper should discuss whether and how consent was obtained from people whose asset is used.
- At submission time, remember to anonymize your assets (if applicable). You can either create an anonymized URL or include an anonymized zip file.

14. **Crowdsourcing and research with human subjects**

Question: For crowdsourcing experiments and research with human subjects, does the paper include the full text of instructions given to participants and screenshots, if applicable, as well as details about compensation (if any)?

Answer: [N/A]

Justification: The paper does not involve crowdsourcing nor research with human subjects.

Guidelines:

- The answer [N/A] means that the paper does not involve crowdsourcing nor research with human subjects.
- Including this information in the supplemental material is fine, but if the main contribution of the paper involves human subjects, then as much detail as possible should be included in the main paper.
- According to the NeurIPS Code of Ethics, workers involved in data collection, curation, or other labor should be paid at least the minimum wage in the country of the data collector.

15. **Institutional review board (IRB) approvals or equivalent for research with human subjects**

Question: Does the paper describe potential risks incurred by study participants, whether such risks were disclosed to the subjects, and whether Institutional Review Board (IRB) approvals (or an equivalent approval/review based on the requirements of your country or institution) were obtained?

Answer: [N/A]

Justification: The paper does not involve crowdsourcing nor research with human subjects.

Guidelines:

- The answer [N/A] means that the paper does not involve crowdsourcing nor research with human subjects.

- Depending on the country in which research is conducted, IRB approval (or equivalent) may be required for any human subjects research. If you obtained IRB approval, you should clearly state this in the paper.
- We recognize that the procedures for this may vary significantly between institutions and locations, and we expect authors to adhere to the NeurIPS Code of Ethics and the guidelines for their institution.
- For initial submissions, do not include any information that would break anonymity (if applicable), such as the institution conducting the review.

16. **Declaration of LLM usage**

Question: Does the paper describe the usage of LLMs if it is an important, original, or non-standard component of the core methods in this research? Note that if the LLM is used only for writing, editing, or formatting purposes and does *not* impact the core methodology, scientific rigor, or originality of the research, declaration is not required.

Answer: [N/A]

Justification: The core method development in this research does not involve LLMs as any important, original, or non-standard components.

Guidelines:

- The answer [N/A] means that the core method development in this research does not involve LLMs as any important, original, or non-standard components.
- Please refer to our LLM policy in the NeurIPS handbook for what should or should not be described.